Sensors and Materials, Vol. 38, No. 8 (2026) 4897–4918
MYU Tokyo

S & M 4601

Digital-twin-based Monitoring and Simulation of S-shaped Tidal Channel in Suncheon Bay, South Korea: Integrated Environmental Data Acquisition and Validation Approach

Jun-Ho Lee,[1,2*] Keunyong Kim,[3] Jingyo Lee,[3] Hwangki Lee,[4] and Hoi-Soo Jung[2]

[1]Korea-Peru Joint Research Center on Ocean Science & Technology for Latin America (KOPELAR), Esquina Gamarra y General Valle s/n, Chucuito, Callao, Callao 07021, Peru
[2]Marine Domain & Security Research Department, Korea Institute of Ocean Science & Technology (KIOST), Busan 49111, Korea
[3]Korea Ocean Satellite Center, Korea Institute of Ocean Science & Technology (KIOST), Busan 49111, Korea
[4]Associated Research Center, Coast and Ocean Technology Research Institute (COTRI), Seoul 08584, Korea

(Received November 24, 2025; accepted August 10, 2026)

Keywords: digital twin, sensor-based monitoring system, environmental sensors, tidal channel, Suncheon Bay

Digital-twin (DT) technology provides a data-driven framework for reproducing complex coastal processes with high spatiotemporal fidelity. In this study, we develop an integrated geospatial digital-twin simulation system (DTSS) for the Suncheon Bay Wetland, an estuarine environment characterized by a pronounced S-shaped tidal channel. High-resolution observations, including sonar-based bathymetry, unmanned aerial vehicle photogrammetric digital elevation models, tidal elevations, current velocity profiles, conductivity temperature depth measurements, and total suspended material time series, were collected during dry (May 2024) and wet (July 2024) seasons and applied to hydrodynamic and salinity-dispersion simulations using the TELEMAC–MASCARET system. The model reproduced semidiurnal tidal behavior under baseflow conditions and captured monsoon-driven effects on river discharge, including delayed ebb–flood transitions and increases in velocity from <0.4 m/s to nearly 1.0 m/s. Salinity simulations revealed sharp gradients during normal flow and near-complete freshwater dominance (<0.1 psu) during peak discharge. Validation metrics [*RMSE*, *BIAS*, and Pearson correlation coefficient ($R > 0.8$)] demonstrated strong agreement between model outputs and observations for tidal elevation, velocity, salinity, and temperature. The DTSS framework effectively integrates sensor-based observations, geospatial data, and numerical modeling, demonstrating how *in situ* sensor networks and DT technologies can be combined to support real-time environmental monitoring, predictive simulations, and intelligent coastal management. These results underscore the importance of river–tide interactions and demonstrate the potential of sensor-driven DT technologies as an integrated platform for real-time wetland monitoring, environmental forecasting, and intelligent coastal management.

*Corresponding author: e-mail: leejh@kiost.ac.kr
https://doi.org/10.18494/SAM6210

1. Introduction

Coastal wetlands are globally recognized as multifunctional ecosystems that provide critical services, including carbon sequestration, biodiversity conservation, shoreline stabilization, nutrient cycling, and buffering against extreme hydrometeorological events. Among these habitats, estuarine tidal flats represent highly dynamic environments where physical processes, including tidal propagation, river discharge, sediment transport, and salinity gradients, interact continuously under the influence of both marine and terrestrial forcings. The complexity of these interactions necessitates advanced methods capable of capturing fine-scale hydrodynamic behavior and its temporal variability. Suncheon Bay Wetland, located along the southern coast of the Korean Peninsula, is one such system where the interplay between tidal currents and freshwater inflow is particularly pronounced.

Suncheon Bay is distinguished by its expansive intertidal flats, extensive reed fields (*Phragmites australis*), and a distinctively sinuous S-shaped tidal channel that functions as a primary conduit for tidal exchange between Yeoja Bay and the Suncheon Dongcheon River.(1) The geomorphological structure and hydrological connectivity of this channel play essential roles in determining sediment pathways, wetland inundation duration, nutrient availability, and habitat zonation. Because this region experiences strong seasonal variability due to monsoon-driven river discharge, tidal forcing is frequently modulated by episodic freshwater inflow that alters water levels, flow asymmetry, and salinity patterns. Understanding such river–tide interactions is thus fundamental for predicting morphological evolution, ecological transitions, and the impacts of climate change on wetland resilience.

Recent technological advances have enabled the application of digital-twin (DT) methodologies to natural environmental systems. A DT is broadly defined as a virtual representation of a physical system that is continuously updated with real-time or periodically acquired data, enabling dynamic monitoring, simulation, and prediction, as described by Grieves.(2) Although originally developed in manufacturing and aerospace engineering, Madni *et al*.(3) gradually expanded DT frameworks to Earth and environmental sciences, offering new opportunities for replicating complex hydrodynamic processes with high spatiotemporal fidelity. When combined with geospatial data such as unmanned aerial vehicle (UAV)-derived digital elevation models (DEMs), sonar-based bathymetry, atmospheric forcing datasets, and *in situ* marine environmental observations, DTs can function as integrated platforms for scenario-based environmental forecasting, resource management, and climate risk assessment.

However, applying DT concepts to coastal wetlands presents several scientific and technical challenges. First, the land–water boundary in tidal flats is highly mobile, requiring submeter-resolution terrain data to accurately capture inundation patterns. Second, estuarine hydrodynamics are governed by nonlinear, depth-averaged shallow-water equations, making numerical simulation sensitive to bathymetric accuracy, boundary conditions, and river discharge variability. Third, salinity, as a conservative scalar influenced by both advection and diffusion, requires high-frequency observational data to properly validate the model. Finally, integrating heterogeneous datasets—including conductivity–temperature–depth (CTD) sensor measurements, UAV photogrammetric DEMs, current-meter observations, and sonar bathymetry—into a unified DT simulation system (DTSS) requires robust geospatial processing and numerical modeling capabilities. The present DTSS represents a DT-ready framework that integrates sensor observations and numerical simulations and is designed to accommodate future real-time data assimilation and automated forecasting capabilities.

Previous studies on Suncheon Bay have been focused on sedimentary processes, ecological distribution, and long-term morphological change, including those by Choi.[1] However, few have attempted a comprehensive approach that simultaneously captures tidal hydrodynamics, river–tide interactions, and salinity dynamics within a single cohesive modeling framework. High-resolution geospatial datasets to calibrate and validate numerical models supporting DT-based applications have been used in even fewer studies. Furthermore, the hydrodynamic and salinity responses of the S-shaped tidal channel—especially under contrasting dry-season and flood-season river discharges—were insufficiently quantified by Passalacqua *et al*.[4] despite their importance to wetland stability, vegetation zonation, and habitat vulnerability.

To address these gaps, in this study, we developed an integrated geospatial DTSS for the Suncheon Bay Wetland by combining extensive field measurements, remote sensing datasets, and numerical simulation tools. High-resolution digital elevation models were constructed using UAV photogrammetry calibrated with real-time kinematic (RTK) ground control points.[5] Sonar surveys provided detailed bathymetric mapping of the S-shaped tidal channel, while water level and current measurements from multiple stations captured tidal variability and river-influenced hydrodynamics during both dry and wet seasons. These datasets were assimilated into the TELEMAC–MASCARET system, a well-established open-source hydrodynamic and transport modeling platform, to simulate tidal propagation, current velocity fields, and salinity dispersion under varying discharge conditions.[6]

Accordingly, the aim of the present study is to establish an integrated DTSS for the Suncheon Bay Wetland by addressing four key objectives. First, we quantify the tidal hydrodynamics in the S-shaped tidal channel under both normal baseflow and monsoon-driven flood-discharge conditions. Second, we evaluate the spatiotemporal characteristics of salinity dispersion under contrasting freshwater inflow scenarios. Third, we assess model accuracy by comparing simulated results with observations using statistical indicators such as root mean squared error ($RMSE$), mean bias error ($BIAS$), and the Pearson correlation coefficient (R). Finally, we demonstrate the applicability of the DTSS framework to real-time environmental monitoring, scenario-based evaluation, and predictive coastal management in estuarine wetlands.

In the context of sensing technology, the present DTSS can be viewed as a virtual extension of the *in situ* sensor network, where tidal gauges, current meters, CTD profilers, and UAV/drone-based platforms are dynamically integrated into a unified monitoring and simulation environment. The framework, therefore, represents a sensor-driven DT platform designed to integrate environmental observations and transform them into predictive information for coastal monitoring and management applications. Through these objectives, the present study provides a scientifically rigorous and sensor-oriented framework that advances the application of DT technologies in coastal research and demonstrates the practical value of environmental sensing systems in estuarine wetlands.

2. Materials and Methods

In this section, we outline the methodological framework used to construct and implement the DTSS for the Suncheon Bay wetland. The procedures encompass geospatial data acquisition, numerical model development, and validation strategies designed to accurately reproduce the hydrodynamic and salinity dynamics of the study area.

2.1 Overall framework of the DTSS

The methodological framework of this study integrates multiscale geospatial data acquisition, hydrodynamic and salinity-transport modeling, and DT-based data assimilation into a unified simulation system tailored for the Suncheon Bay Wetland (mud flats) in Fig. 1. The DTSS was developed as a modular environment capable of ingesting diverse datasets, including bathymetry, tidal elevations, atmospheric forcing, river discharge, and water-column observations, to continuously refine the numerical representation of the wetland. The overall architecture follows a three-stage workflow consisting of (1) geospatial data acquisition and preprocessing, (2) numerical model construction and simulation, and (3) statistical model validation. This structure is consistent with recent DT-oriented environmental platforms for estuaries and coastal wetlands

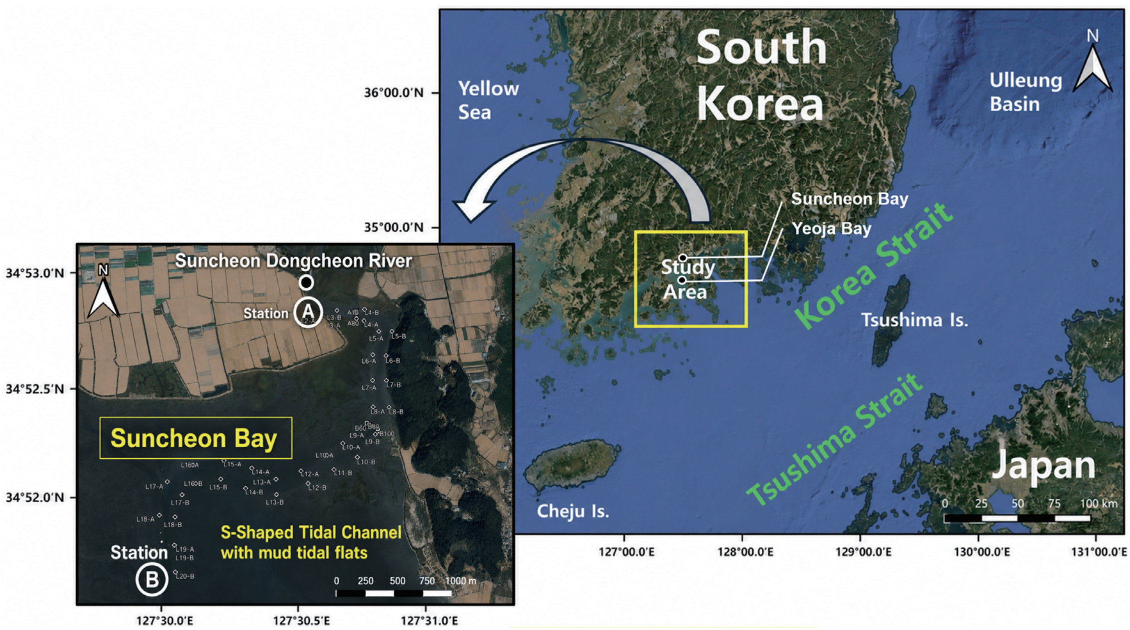

Fig. 1. (Color online) Location of the study area on the South Korean Peninsula and an enlarged view of Suncheon Bay showing the S-shaped tidal channel, surrounding mud flats, and monitoring stations.

described by Neal *et al*.[7] and, owing to its modularity, can be readily expanded to incorporate sediment-transport modules, ecological indicators, or machine-learning-based forecasting tools in future applications.

2.2 Study area and hydrological forcing characteristics

Suncheon Bay is a mesotidal estuarine environment with semidiurnal tidal cycles and pronounced monsoon-driven hydrological variability. The wetland's S-shaped tidal channel plays a central role in controlling energy dissipation, freshwater mixing, sediment pathways, and inundation patterns. The Suncheon Dongcheon River, located immediately upstream, provides freshwater discharge that varies seasonally from ~2.3 m^3/s during the dry season to >200 m^3/s during peak rainfall events. This large hydrological gradient creates strong contrasts in tidal propagation, flow asymmetry, and stratification, making the system ideal for DT-based hydrodynamic simulation.

Bathymetrically, the region features shallow intertidal flats with elevations ranging from −1.5 to +1.8 m relative to mean sea level, intersected by a deeply incised tidal channel. The geomorphic structure amplifies river–tide interactions, often modifying flood-tide penetration and ebb-tide flushing. Given these characteristics, detailed observations of the terrain and water column were necessary to accurately reconstruct the coastal system.

2.3 Field data acquisition (tidal elevation, current, and river discharge)

A multistation observational approach was implemented to characterize tidal elevation and current dynamics during both the dry season (May 2024) and the wet season (July 2024). Three fixed monitoring stations, A, B-1, and B-2, were deployed during both the baseflow (May, dry season) and flood (July, flood season) seasons to measure tidal elevation, horizontal flow velocity, and CTD parameters. Station A, located near Mujin Bridge, provided long-term tidal records spanning over 30 days for both seasons, while Station B-1 recorded tidal elevation and current patterns during the dry season, and Station B-2 captured tidal elevation, current velocity, salinity, and temperature during the wet season. Horizontal current measurements were obtained using recording current meters (RCMs), which provided high-temporal resolution vector velocity data. CTD profiles were collected during both neap and spring tidal cycles to assess vertical stratification. All sensors were calibrated prior to deployment using standard reference solutions for conductivity and temperature to ensure measurement accuracy.

River discharge plays a primary role in controlling estuarine hydrodynamics; therefore, the accurate estimation of discharge from Suncheon Dongcheon was essential. Discharge was estimated using Eq. (1).

$$Q = A \cdot U \tag{1}$$

Q = discharge (m^3/s)
A = cross-sectional area (m^2)
U = depth-averaged velocity (m/s)

RTK-surveyed transects and acoustic depth measurements were used to determine the cross-sectional geometry of the channel at Mujin Bridge, while velocity distributions were obtained from CTD and RCM measurements in Figs. 2 and 3. On the basis of these observations and existing hydrological records, the baseflow discharge was set to 2.337 m^3/s, as per the Suncheon River Master Plan, and the flood-season discharge was set to 219.4 m^3/s, representing the 5-year mean annual peak reported by WAMIS.[8] These discharge values were applied as upstream inflow boundary conditions in the TELEMAC model.

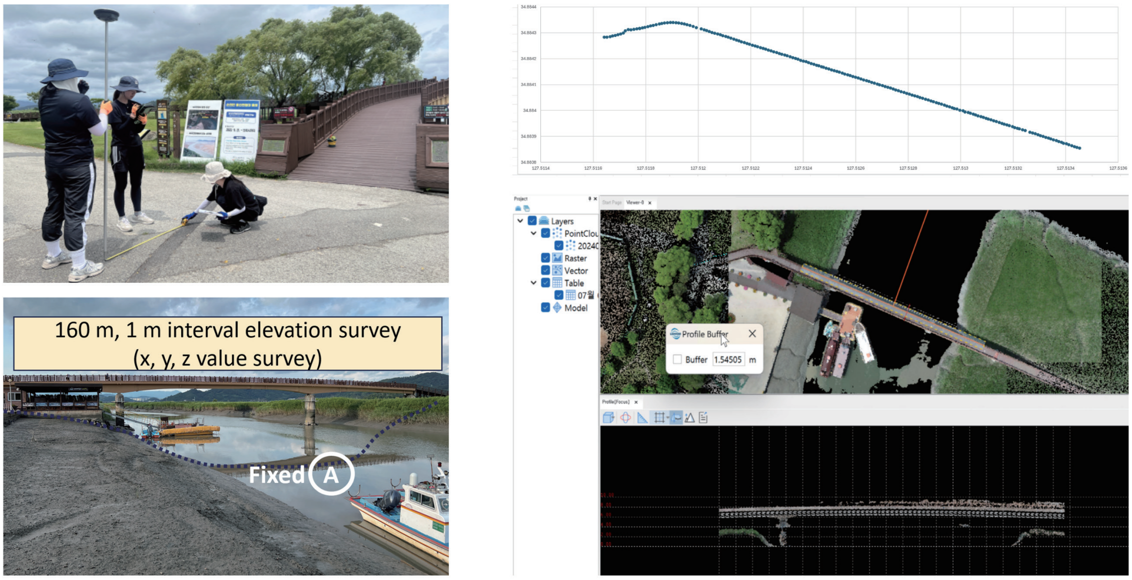

Fig. 2. (Color online) From the second field survey results, an elevation profile of approximately 160 m at Mujin Bridge (1 m intervals) was obtained and cross-compared with drone LiDAR point cloud data and RTK measurement.

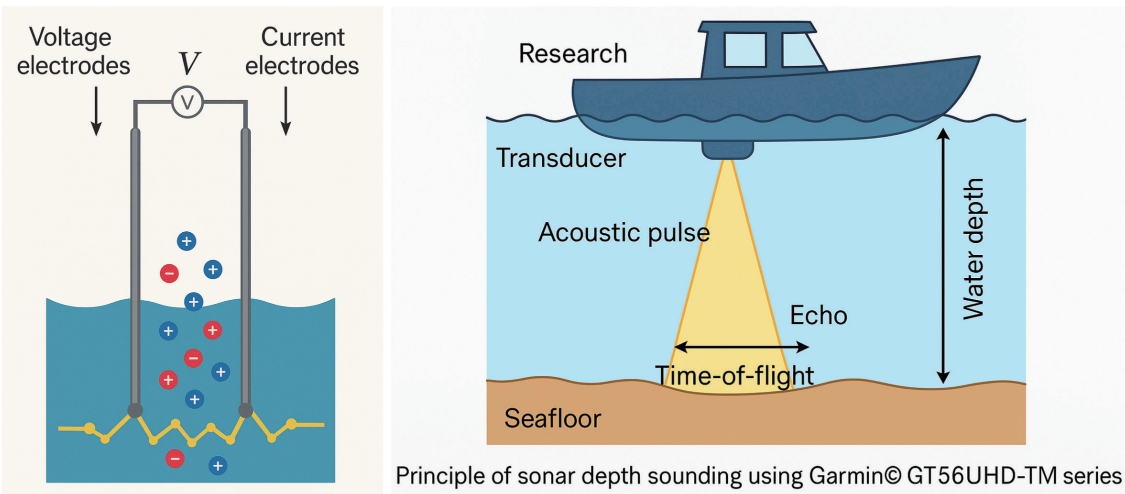

Fig. 3. (Color online) Measurement principles of the CTD (YSI© EXO series) sensor for salinity data and configuration diagram of the SONAR research equipment (Garmin© GT56UHD-TM series) used for *in situ* depth sounding.

2.4 High-resolution terrain construction (UAV photogrammetric DEM, sonar-based bathymetry)

UAV photogrammetry was performed using a calibrated camera system equipped with known interior orientation parameters (IOPs). Ground control points (GCPs) were surveyed using Network-RTK, achieving sub-centimeter horizontal and vertical precisions. Structure-from-motion (SfM) bundle adjustment was applied to generate dense point clouds, followed by orthomosaic and DEM construction.[5,9] DEM accuracy was validated against RTK survey points, yielding a vertical *RMSE* of a few millimeters for the area shown in Fig. 2.

Sonar data were collected using a Garmin GT56UHD-TM ultrahigh-definition transducer. A total of 44837 pings were acquired, with 2211 validated after filtering out oblique angles, positional errors, and noise, as shown in Figs. 3 and 4. The final bathymetry covered the full

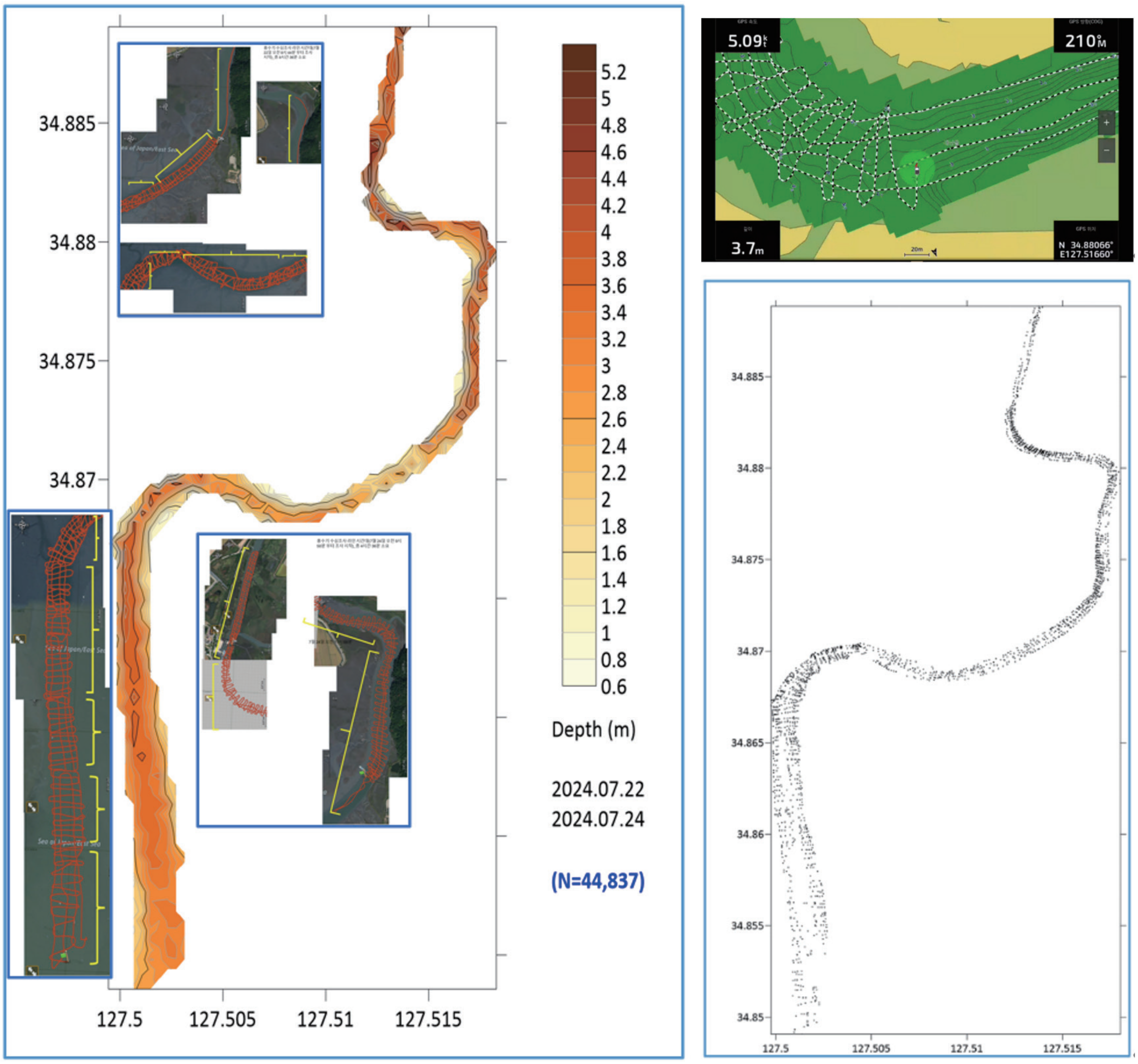

Fig. 4. (Color online) Survey vessel track lines and bathymetric contour intervals showing the total number of acquired pings (44837) and the final dataset used for model implementation and simulator enhancement (2211 pings).

extent of the S-shaped channel. These points were merged with the UAV DEM to create a fused hybrid terrain model, ensuring seamless representation of the intertidal and subtidal zones in Fig. 2.

2.5 Numerical model setup

Hydrodynamic and salinity-dispersion simulations for the Suncheon Bay wetland were performed using a depth-averaged numerical modeling framework that had been independently validated through extensive field observations. Verification data included tidal elevation, current velocity, salinity, and water temperature collected at Stations A, B-1, and B-2 during both the baseflow (May, dry season) and flood (July, flood season) seasons.[10,11] Model–observation agreement was quantitatively evaluated using the previously provided error metrics. The absolute relative error (*ARE*) was computed, as shown in Eq. (2).

$$ARE(\%) = \frac{|M_i - O_i|}{|O_i|} \times 100, \; Error = Modeled - Observed \tag{2}$$

Here, M_i = modeled value at index i, and O_i = observed value at index i.

The mean squared error (*MSE*) is calculated as shown in Eq. (3).

$$MSE = \frac{1}{N}\sum_{i=1}^{N}(y_i - \widehat{y_i})^2 \tag{3}$$

Here, N = number of data points, y_i = observed value (actual value), and $\widehat{y_i}$ = modeled value (predicted value).

RMSE is determined as

$$RMSE = \sqrt{\sum_{i=1}^{N}\frac{(\widehat{y_i} - y_i)^2}{N}}. \tag{4}$$

The mean bias error (*BIAS*) is

$$BIAS = \left(E\left[\widehat{y_i} - y_i\right]\right). \tag{5}$$

Here, E is expectation. A positive *BIAS* indicates that the predicted values are systematically higher than the observed values (overestimation), and a negative *BIAS* indicates that the predicted values are systematically lower than the observed values (underestimation).

The Pearson correlation coefficient (R) is as shown in Eq. (6).

$$R = \frac{\operatorname{cov}\left(\widehat{y_i}, y_i\right)}{\sqrt{\operatorname{var}\left(\widehat{y_i}\right)\operatorname{var}\left(y_i\right)}} \tag{6}$$

These statistical indicators provided a consistent framework for assessing the predictive skill and determining the suitability of the model for hydrodynamic and scalar-field simulations, based on the evaluation method proposed by Willmott.(12)

Tidal forcing at the open boundary was imposed using 16 harmonic constituents, while freshwater inflow from Suncheon Dongcheon was applied at the upstream boundary using observed river-discharge records. Atmospheric variables required for surface heat and salinity exchange—including wind speed, temperature, humidity, cloud cover, and meteorological data—were obtained from the Korea Meteorological Administration (KMA) Automatic Weather Station (AWS). Oceanographic data were acquired from the Korea Hydrographic and Oceanographic Agency (KHOA) ocean buoy network. Boundary conditions were supplemented using the HYCOM reanalysis product.

A uniform computational time step of 1 s was used, and the same computational grid was applied to both hydrodynamic and salinity simulations to maintain numerical consistency.(13) Model calibration and validation were performed separately for the baseflow period (16–22 May 2024) and the flood period (24 June–23 July 2024). The validated model achieved high predictive performance, with correlation coefficients generally exceeding 0.90 and low *RMSE* values for tidal elevation and salinity. These results confirm that the model is sufficiently robust to simulate tidal currents and salinity dispersion processes across the Suncheon Bay intertidal system.

2.6 Salinity transport simulation

The salinity-dispersion simulation was conducted on the same grid and with the same temporal resolution as the hydrodynamic model to ensure a consistent numerical framework between momentum and scalar transport. Freshwater inflow from Suncheon Dongcheon and saline intrusion from Yeoja Bay acted as the primary forcing mechanisms controlling salinity distribution within the S-shaped tidal channel. Boundary salinity values were prescribed using *in situ* CTD measurements collected at Stations B-1 (dry season) and B-2 (flood season). Offshore boundary conditions were complemented by HYCOM reanalysis fields to represent regional water-mass characteristics during the study period.

Model performance was evaluated using the previously defined verification metrics (*ARE*, *MSE*, *RMSE*, *BIAS*, and *R*). During the dry season, the simulation yielded an *RMSE* of 2.79 psu and a correlation coefficient of 0.94 at B-1, indicating strong agreement between observed and modeled salinity fluctuations. Under flood-season conditions, an *RMSE* of 1.84 psu with R = 0.92 was obtained at B-2, demonstrating that the model effectively reproduced the significant freshwater flushing and the associated decrease in salinity gradients during high-discharge events.

The baseflow and flood seasons required separate simulations because of the substantial differences in the hydrologic regime. During the dry season, saline intrusion and ebb–flood salinity asymmetry were clearly reproduced, whereas the flood season was characterized by persistent near-freshwater conditions (<0.1 psu) across most of the tidal creeks. The model successfully simulated these contrasting salinity structures, confirming its ability to capture both tidal mixing and river-dominated stratification, which are common to estuarine wetlands.

2.7 Statistical validation

Statistical validation of the numerical model was conducted by comparing simulated water levels, current velocities, salinities, and temperatures with corresponding field observations from Stations A, B-1, and B-2. The same set of previously defined quantitative indices—*MSE*, *RMSE*, *BIAS*, and *R*—were used without redefining their mathematical expressions, thereby ensuring consistent comparison across hydrodynamic and scalar processes.(13)

For tidal elevation, correlation coefficients at all stations exceeded 0.90, demonstrating excellent alignment between modeled and observed tidal oscillations during both dry and flood seasons. Current-velocity validation similarly demonstrated high performance, with *R* values ranging from 0.87 to 0.93, indicating the accurate reproduction of both the magnitude and phase of tidal currents.

Salinity and temperature validation at B-1 and B-2 also produced strong agreement, with correlation coefficients of 0.91–0.94 and low *BIAS* values. These results confirm that the model effectively captures freshwater intrusion, tidal flushing, thermal variability, and stratification patterns.

Consistent with widely accepted estuarine modeling standards, correlation coefficients greater than 0.80 were interpreted as indicating strong model-observation agreement. All simulated variables in this study exceeded this threshold under both dry-season and flood-season conditions, demonstrating the reliability of the integrated hydrodynamic–salinity modeling framework for application to the Suncheon Bay wetland.

3. Results

In this section, we present the hydrodynamic responses of the Suncheon Bay Wetland under contrasting seasonal conditions, highlighting key differences between the dry and wet periods.

3.1 Overview of hydrodynamic response under contrasting seasonal conditions

Hydrodynamic simulations for the Suncheon Bay Wetland revealed pronounced differences between dry-season (May) and wet-season (July) conditions, driven primarily by variations in river discharge from the Suncheon Dongcheon River. During the dry season, the estuarine system exhibited a predominantly tidally driven flow regime with stable semidiurnal cycles. In contrast, the wet season exhibited significantly altered hydrodynamics owing to strong monsoon-induced freshwater discharge, which modulated tidal propagation, water level variations, flow velocities, and salinity distributions. The combined analysis of tidal elevation, current velocity, flow direction, and scalar transport provides a comprehensive understanding of the physical processes governing the S-shaped tidal channel.

3.2 Tidal elevation characteristics

During the dry season (May 16–25, 2024), observed and simulated tidal elevations exhibited consistent semidiurnal patterns with moderate tidal ranges, with high tide reaching approximately 214 cm and low tide dropping to −119 cm relative to mean sea level (MSL), as seen in Fig. 5. Tidal curves at Stations A and B-1 displayed clear diurnal inequality, characterized by alternating higher high tides and lower low tides, consistent with the dominant regional tidal constituents along the southern coast of Korea. Model–observation comparisons for this period showed strong agreement, with correlation coefficients of $R \geq 0.9$, *RMSE* values generally below 5–7 cm, and minimal *BIAS*, confirming the model's ability to reproduce both the magnitude and timing of tidal elevations under low river discharge conditions. In contrast, during the wet season (June 23–July 31, 2024), tidal dynamics diverged from those of the dry season owing to elevated river discharge, which reached up to 219.4 m^3/s. While high tide remained comparable to dry-season levels (~214 cm), low tide did not return to its typical elevation, indicating a backwater effect due to sustained freshwater inflow. This effect was most evident at Station A, the upstream location, where water levels remained elevated across multiple tidal cycles, reflecting reduced tidal asymmetry and a muted ebb-phase recession. Despite greater hydrologic variability and localized turbulence during peak discharge conditions, model–observation correlations during the wet season remained strong ($R \geq 0.8$), although *RMSE* values increased slightly relative to the dry season.

3.3 Current velocity and flow structure

Under baseflow conditions, the S-shaped tidal channel functioned as a tidally dominated conduit, with relatively weak peak flood velocities of approximately 0.1 m/s in the Station A mobile transects and ~0.4 m/s at the B fixed barge station, while peak ebb velocities reached ~0.2 m/s at A and ~0.4 m/s at B. Velocity vectors showed flood currents entering from the south

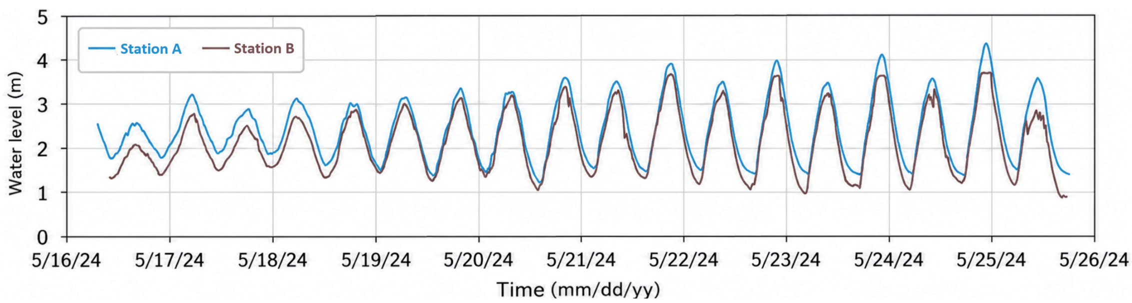

Fig. 5. (Color online) Tidal variations at Station A (fixed, Mujin Bridge) and Station B-1 [May, dry season, fixed unmanned vessel (UV)].

(Yeoja Bay) and propagating northward toward the interior of the wetland, whereas ebb flows reversed direction and moved southward along the main tidal creek. Spatial analysis of model outputs revealed distinct acceleration zones within constricted sections and deceleration zones near channel–flat transition areas, indicating tendencies toward erosion in narrow bends and sediment deposition in wider channel reaches. During wet-season flood discharge events, however, the estuary's hydrodynamic behavior changed dramatically, as seen in Figs. 6 and 7.

Increased river discharge delayed the onset of the flood tide, preventing the immediate reversal of ebb flow and producing prolonged seaward currents during the transitional phases. Maximum velocities in the northern channel increased substantially, reaching ~1.2 m/s during flood tide and up to ~1.6 m/s during ebb tide at Station A. Strong freshwater forcing also produced persistent unidirectional flow, with seaward-directed vectors observed even during the nominal flood tide in the upper channel. In contrast, the southern channel (B-sector) maintained a stronger tidal influence owing to its proximity to the tidal inlet, with peak velocities remaining in the 0.6–0.9 m/s range—similar to dry-season conditions—highlighting its tidal dominance. These contrasting responses underscore the spatial heterogeneity of river–tide interactions

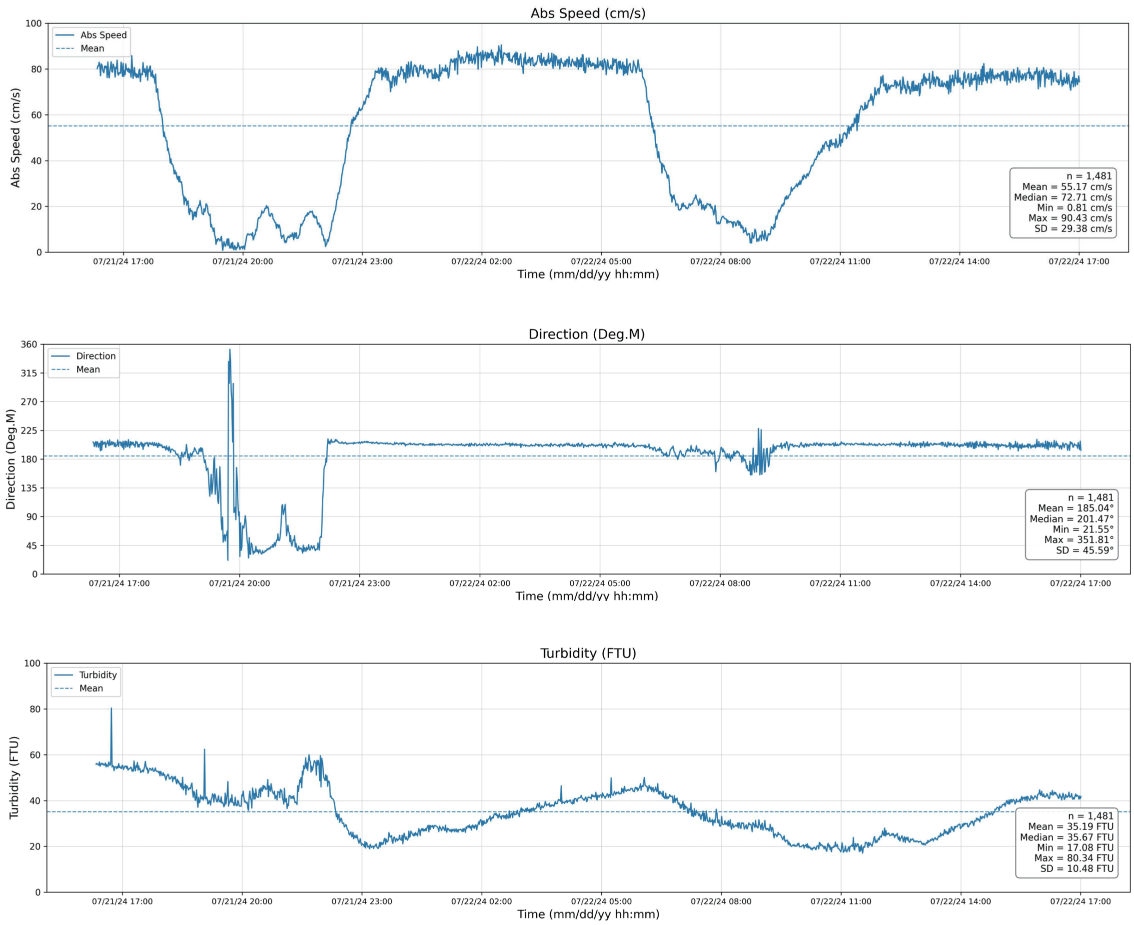

Fig. 6. (Color online) Station A (July, flood season, fixed UV) near Mujin Bridge: acquisition of physical data including current direction, current velocity, and turbidity (Formazin Turbidity Unit, FTU) over 24 hours.

Fig. 7. (Color online) Station B-2 (July, flood season, fixed UV) time-series measurements of surface current velocity (speed), current direction, turbidity, salinity, and temperature; 16-day continuous physical dataset acquired.

within the system, with the upper channel exhibiting river-dominated hydraulics during flood discharge and the lower channel retaining the characteristic tidal signatures shown in Figs. 6 and 7.

3.4 Spatial and temporal distribution of salinity (dry and flood season salinity patterns)

Under baseflow conditions, salinity distributions exhibited sharp but predictable gradients, with flood-tide salinity reaching ~5 psu in the S-shaped creek and ~29 psu in the southern channel, while ebb-tide values dropped to ~0.1 and ~3 psu, respectively, indicating partial saline intrusion during flood periods but strong freshwater influence upstream during ebb phases. The salinity interface migrated dynamically with the tidal cycle, and model results closely matched CTD observations at Station B-1, yielding an *RMSE* of 2.79 psu, a near-zero *BIAS* (−0.03), and a correlation coefficient of $R = 0.94$, as shown in Table 1 and Figs. 8 and 9.

In contrast, flood-season discharge considerably altered the salinity structure: on Day 1, flood-tide salinity remained at ~0.1 psu in the S-shaped creek and ~25 psu in the southern channel, while ebb-tide values dropped to <0.1 and ~0.2 psu. By Day 2, most of the tidal channel exhibited near-complete freshwater dominance (<0.1 psu). This pronounced downstream displacement of the salinity front demonstrates the strong suppression of saline intrusion under high-discharge conditions, resulting in reduced seawater residence time and substantially modified biogeochemical environments, as shown in Table 1 and Figs. 8 and 10.

Table 1
Validation results of salinity and temperature during dry (B-1) and wet (B-2) seasons.

Seasons (Station)	Variable (salinity: psu temperature: °C)	*RMSE* (root mean square error)	*BIAS* (mean bias error)	*R* (–) (correlation coefficient)
Dry season (Station B-1)	Salinity temperature	2.79 1.74	−0.03 −0.89	0.94 0.93
Flood season (Station B-2)	Salinity temperature	1.84 3.03	0.02 −1.04	0.92 0.91

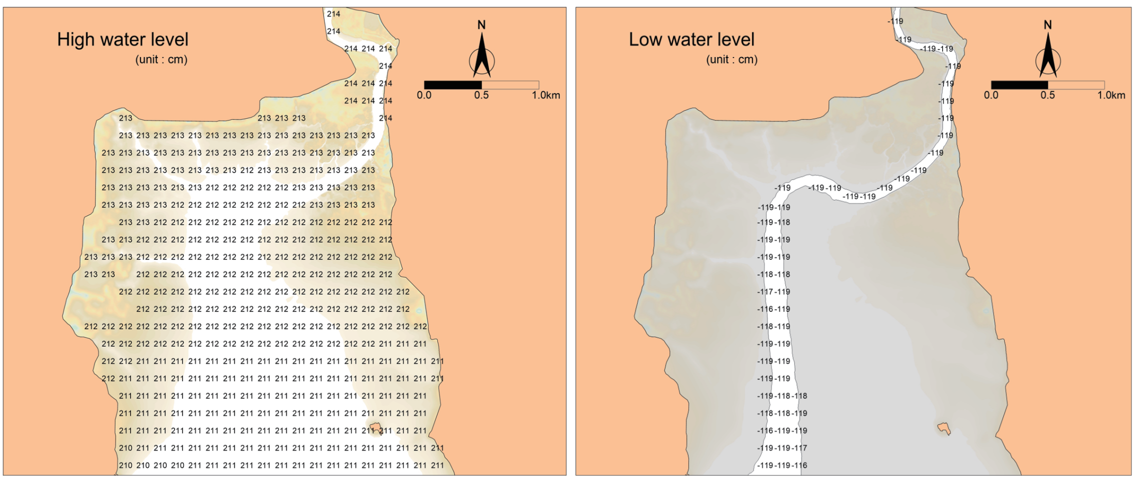

Fig. 8. (Color online) Distribution at high and low tide under normal-flow conditions.

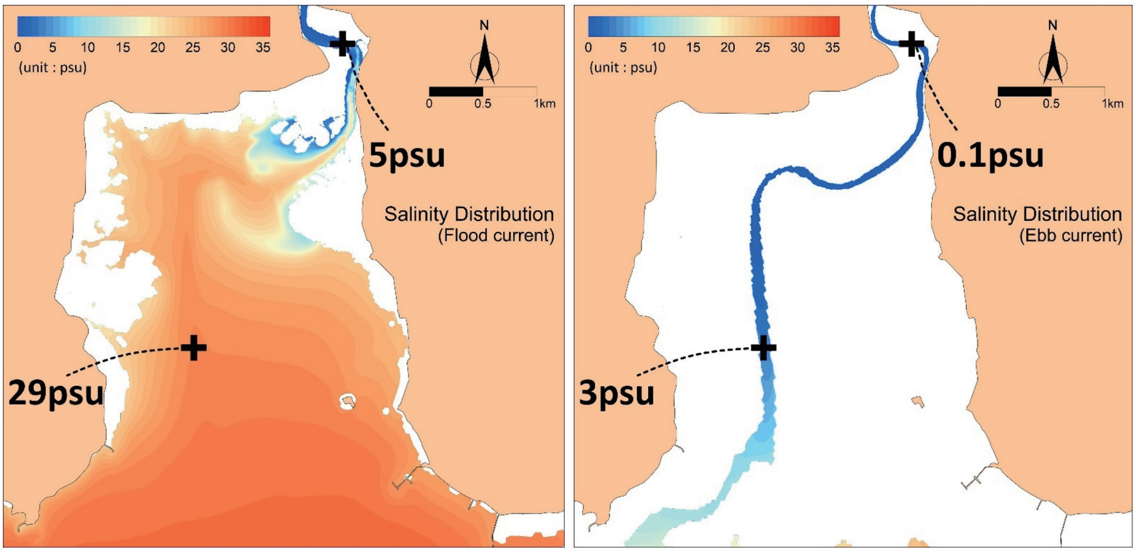

Fig. 9. (Color online) Salinity distribution during flood and ebb tides at spring tide (Suncheon Bay wetland in the dry season).

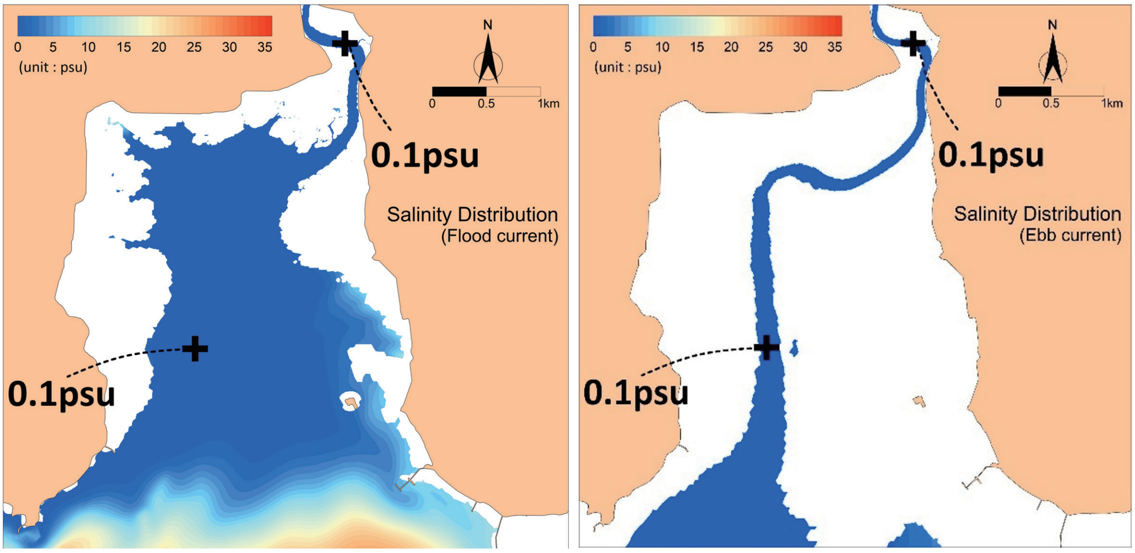

Fig. 10. (Color online) Salinity distribution during flood and ebb tides under spring-tide conditions (Suncheon Bay wetland, day 2 of the flood season during the monsoon).

3.5 Model performance and validation

Model validation against field observations demonstrated high accuracy across hydrodynamic and salinity parameters. For tidal elevation, the model achieved *RMSE* values of ≤7 cm during the dry season and ≤10 cm during the wet season, with correlation coefficients of $R \geq 0.9$ and

$R \geq 0.8$, respectively. Current velocity comparisons also showed strong agreement in the dry season, with only slight deviations during peak flood discharge. Increased turbulence contributed to minor discrepancies, although correlation values consistently exceeded 0.8. Salinity validation yielded *RMSE* values ranging from 0.5 to 3.0 psu, depending on the station and season, with *BIAS* values near zero, and correlation coefficients reaching $R \geq 0.91$ at Station B-2 during the wet season for combined temperature and salinity datasets. Together, these metrics confirm that the DT-supported TELEMAC model reliably reproduces the hydrodynamic and salinity dynamics of Suncheon Bay under both tidal-dominated and flood-dominated conditions.

4. Discussion

In this section, we interpret the hydrodynamic and salinity responses revealed by the simulations, with particular emphasis on the physical mechanisms governing tidal behavior and river–tide interactions in the S-shaped channel.

4.1 Hydrodynamic controls in S-shaped tidal channel and river–tide interaction dynamics

The hydrodynamic simulations conducted in this study reveal that the S-shaped tidal channel of the Suncheon Bay Wetland is governed by a dynamic balance between tidal forcing at the southern open boundary and freshwater discharge from the Suncheon Dongcheon River at the northern boundary. Under dry-season conditions, the estuary behaves as a classical mesotidal system dominated by semidiurnal tides, with flood currents propagating northward and ebb currents reversing southward in a predictable bidirectional exchange. These patterns align with estuarine flow structures described in previous studies, where tidal asymmetry and channel sinuosity generate localized zones of acceleration and deceleration.(6,13) However, during wet-season monsoon events, this balance shifts dramatically owing to increased river discharge, which alters the timing, magnitude, and spatial structure of tidal propagation. The numerical results demonstrate a delayed transition from ebb to flood flow, a well-documented phenomenon in systems where freshwater inflows exert a backwater effect capable of temporarily suppressing incoming tidal energy.(14,15) In Suncheon Bay, this delay was most pronounced at Station A, where elevated water levels persisted over several cycles, indicating that the estuary temporarily adopted a river-dominant hydraulic regime.

Peak velocities increased sharply—by up to 4–6 times compared with dry-season values—in constricted segments of the S-shaped channel. This shift indicates an increase in shear stress and a potential for sediment mobilization during the wet season, consistent with observations from other monsoon-influenced estuaries in East Asia.(16) In contrast, the lower channel (Station B) retained strong tidal influence, demonstrating a spatial partitioning between tidal- and discharge-dominated subregions. The coexistence of these regimes highlights the geomorphic significance of channel sinuosity, width variability, and estuarine bathymetry in influencing tidal resonance and flow resistance.

Furthermore, the model successfully reproduced the inability of low tides to fall below a critical elevation during peak discharge. Such behavior indicates the formation of a hydraulic "buffer layer" created by sustained river inflow, which prevents full tidal recession. This phenomenon has significant implications for wetland inundation duration, exposure intervals, and sediment deposition, suggesting that river discharge may serve as a short-term stabilizing mechanism that limits the desiccation of upper tidal flats.[9]

4.2 Spatiotemporal dynamics of salinity dispersion and freshwater influence

Salinity patterns in Suncheon Bay reflect the strong interaction between tidal mixing and freshwater flushing. During the dry season, salinity gradients exhibited classical estuarine behavior, with saline intrusion penetrating the mid-channel during the flood tide and retreating seaward during the ebb tide. The presence of ~5 psu water in the S-shaped segment and ~29 psu water in the southern channel during flood conditions indicates partial but limited saline intrusion, modulated by bathymetric constraints and channel sinuosity. These gradients are consistent with theoretical models of estuarine circulation, where channel curvature and bed friction reduce the landward progression of salt wedges, as described by Dyer[14] and Ruhl and Schoellhamer.[17]

In contrast, during wet-season flood discharge, salinity dropped below 0.1 psu across extensive areas, especially in the upper and mid-channel regions. The rapid decline in salinity reflects strong advection-dominated transport, with freshwater overwhelming tidal intrusion. The persistence of <0.1 psu salinity over two consecutive days further emphasizes the estuary's sensitivity to monsoon-driven inflows.[18] Morris *et al*.[15] showed that such freshwater pulses alter phytoplankton composition, nutrient availability, and benthic organism survival in numerous estuarine systems.

The numerical model's ability to replicate these salinity dynamics, with correlation coefficients of $R \geq 0.9$ at B-1 and B-2, demonstrates effective representation of both advective and diffusive processes within TELEMAC's scalar transport module. The model's reliability under varying hydrological conditions underscores its suitability for long-term ecological forecasting and water-quality management. For instance, the extended period of freshwater dominance during flood conditions suggests a temporary reduction in salinity stress for reed communities (*Phragmites australis*), while potentially adverse conditions may occur for halophytes such as *Salicornia*. Such prolonged freshwater conditions may affect benthic macrofauna, including bivalves and polychaetes adapted to brackish environments. Rapid reductions in salinity can alter species composition, recruitment success, and nutrient cycling processes within the wetland ecosystem.

4.3 Implications for wetland morphodynamics and sediment transport

Although sediment transport was not explicitly simulated in this study, the observed hydrodynamic and salinity patterns yield valuable insights into potential morphodynamic responses of Suncheon Bay's tidal flats. The significant increase in current velocity during flood-season discharge implies enhanced sediment mobility, especially within constricted reaches of the S-shaped channel where bed shear stress is amplified. Studies of meandering tidal channels have shown that such increases in discharge-driven velocity accelerate channel deepening, bank erosion, and point-bar migration.(1,4,16,19) The spatial differentiation between the river-influenced upper channel and the tide-dominated lower channel suggests a heterogeneous sediment regime, with possible deposition zones near channel mouths where velocities suddenly decrease.

Persistent freshwater dominance during monsoon periods may also affect the residence time of suspended sediments. Under dry-season conditions, saline intrusion increases water density and stratification, reducing vertical mixing. However, under flood-season conditions, strong freshwater flushing likely increases the export of fine suspended sediments seaward. This dynamic may reduce sediment availability for marsh accretion, potentially influencing long-term stability of the wetland under the projected sea-level rise.

4.4 Performance and advantages of DTSS

The DTSS developed in this study integrates hydrodynamic modeling, field measurements, and geospatial terrain data into a unified and flexible platform, demonstrating high reliability across varying environmental conditions, as evidenced by strong validation metrics such as *RMSE*, *BIAS*, and *R*. Its strengths include the ability to assimilate multisource datasets—including UAV-derived DEMs, sonar bathymetry, CTD profiles, and current measurements—to operate effectively under rapidly changing hydrological conditions, provide scenario-based predictions for flood events, sea-level rise, and habitat responses, and offer scalable opportunities for real-time data integration. Unlike conventional models, the DTSS employs an adaptive architecture that can be continuously updated as new observations become available, thereby enhancing its predictive skill over time. Such adaptability has been recognized as essential for managing environmentally vulnerable estuaries under climate change and anthropogenic stress.(3,6) In the context of Suncheon Bay, this capability translates into the improved prediction of wetland exposure and inundation duration, the identification of vulnerable zones under sea-level rise, enhanced support for reed-zone conservation strategies, better anticipation of hydrodynamic shifts during extreme rainfall events, and the provision of robust scientific evidence to guide estuarine restoration and engineering decisions.

4.5 Broader implications for coastal management and future DT applications

Our findings in this study underscore the importance of considering river discharge variability when managing estuarine wetlands. In Suncheon Bay, the stark differences between dry- and wet-season hydrodynamics reveal that simplistic tidal-only models are insufficient for accurate environmental planning. The DTSS approach demonstrates the feasibility and necessity of integrating high-resolution terrain data with physically based numerical models to produce reliable, real-time or near-real-time monitoring tools. An example is shown in Fig. 11.

Fig. 11. (Color online) EGIS Inc. utilized a three-dimensional hydrodynamic SaaS-based numerical simulation model to conduct seawater circulation and salinity-dispersion simulations under both normal-flow and flood-season conditions in the Suncheon Bay estuary.[20]

In the context of climate change, these insights are critical. Increased rainfall variability, more frequent extreme discharge events, and accelerating sea-level rise are expected to reshape estuarine processes globally. DT technologies offer a pathway to anticipate such transformations by simulating future scenarios, evaluating intervention strategies, and supporting adaptive ecosystem-based management.

Future enhancements to the Suncheon Bay DTSS can include sediment-transport modules, real-time sensor networks, ecological modeling components, or machine-learning-based predictive analytics. The modular nature of DTSS ensures that the system can evolve from a hydrodynamic simulator to a multilayered environmental intelligence platform. The present simulations assumed static bathymetry between May and July. Although no major geomorphic changes were observed during the study period, localized erosion and deposition during peak discharge events may introduce additional uncertainty in flow and salinity simulations.

5. Conclusions

We developed a comprehensive geospatial DTSS for the Suncheon Bay Wetland by integrating high-resolution field observations, UAV-derived photogrammetric terrain models, sonar-based bathymetry, and numerical simulations with the TELEMAC–MASCARET system. The combined evaluation of hydrodynamics and salinity dispersion across contrasting seasonal conditions highlighted the strong influence of river discharge on tidal propagation, flow velocity, and saline intrusion within the S-shaped tidal channel.

During the dry season, Suncheon Bay exhibited a typical semidiurnal tidal regime with predictable flood–ebb transitions and moderate salinity gradients. However, during the wet season, monsoon-driven discharge significantly altered the hydrodynamic behavior, delaying tidal reversals, increasing peak velocities to nearly 1 m/s, and suppressing low-tide water recession. Salinity dispersion patterns further revealed that freshwater inflow can dominate the entire tidal creek network, reducing salinity to <0.1 psu over multiple tidal cycles. Model validation using *RMSE*, *BIAS*, and *R* demonstrated excellent agreement between simulations and observations ($R \geq 0.8$ for all major variables), confirming the accuracy and robustness of the DTSS framework.

The findings underscore several key implications.

(1) Seasonal river discharge exerts a critical control over tidal hydrodynamics, influencing habitat distribution, sediment transport potential, and inundation patterns.

(2) The S-shaped tidal channel exhibits spatial partitioning between river- and tide-dominated subregions, with potential consequences for sedimentary processes and ecological zonation.

(3) DT approaches offer a powerful and scalable tool for real-time monitoring, scenario evaluation, and long-term coastal-wetland management.

(4) Although real-time IoT-based synchronization was not implemented in the present study, the modular architecture of the DTSS enables future integration of real-time sensor streams.

The present framework demonstrates how sensor-driven DT technologies can support environmental monitoring, predictive simulations, and decision-making processes by continuously integrating observations from tidal gauges, CTD sensors, current meters, and UAV-based geospatial platforms. This study, therefore, provides an operational example of how advanced sensing technologies can be combined with numerical modeling to establish intelligent environmental monitoring systems for coastal wetlands. This study also provides a foundational DT infrastructure for the Suncheon Bay Wetland and establishes a methodological template that can be extended to other estuarine systems facing hydrodynamic complexity and climate-driven uncertainty. Future research should integrate sediment transport, ecological response modeling, and real-time sensor networks to enhance the predictive capability and operational utility of the DT platform. This sensor-integrated DT framework provides a promising pathway toward next-generation smart coastal observatories and real-time environmental intelligence systems.

Acknowledgments

This research was supported by the Korea Institute of Marine Science & Technology Promotion (KIMST) funded by the Ministry of Oceans and Fisheries (RS-2023-00254717). This work was also supported by the Korea Institute of Ocean Science & Technology (2520000770).

References

1 K. Choi: Ocean Coast. Manage. **102** (2014) 437. https://doi.org/10.1016/j.ocecoaman.2014.07.009
2 M. Grieves: Digital Twin: Manufacturing Excellence through Virtual Factory Replication (2014). https://www.3ds.com/fileadmin/PRODUCTS-SERVICES/DELMIA/PDF/Whitepaper/DELMIA-APRISO-Digital-Twin-Whitepaper.pdf (accessed June 2026).
3 A. M. Madni, C. C. Madni, and S. D. Lucero: Systems **7** (2019) 7. https://doi.org/10.3390/systems7010007
4 P. Passalacqua, S. Lanzoni, C. Paola, and A. Rinaldo: J. Geophys. Res. Earth Surf. **118** (2013) 1838. https://doi.org/10.1002/jgrf.20128

5 M. J. Westoby, J. Brasington, N. F. Glasser, M. J. Hambrey, and J. M. Reynolds: Geomorphology **179** (2012) 300. https://doi.org/10.1016/j.geomorph.2012.08.021
6 J.-M. Hervouet: Hydrodynamics of Free Surface Flows: Modelling with the Finite Element Method (John Wiley & Sons, Chichester, 2007). https://doi.org/10.1002/9780470319628
7 J. Neal, G. Schumann, and P. Bates: Water Resour. Res. **48** (2012) W11506. https://doi.org/10.1029/2012WR012514
8 WAMIS (Water Resources Management Information System): Annual Hydrologic Data for Suncheon Dongcheon (2023) (in Korean) https://www.wamis.go.kr (accessed June 2026).
9 M. A. Fonstad, J. T. Dietrich, B. C. Courville, J. L. Jensen, and P. E. Carbonneau: Earth Surf. Process. Landf. **38** (2013) 421. https://doi.org/10.1002/esp.3366
10 A. Malcherek: Hydrol. Process. **14** (2000) 2293. https://doi.org/10.1002/1099-1085(200009)14:13<2293::AID-HYP29>3.0.CO;2-4
11 S. D. Sandbach, A. P. Nicholas, P. J. Ashworth, J. L. Best, C. E. Keevil, D. R. Parsons, E. W. Prokocki, and C. J. Simpson: Estuar. Coast. Shelf Sci. **212** (2018) 176. https://doi.org/10.1016/j.ecss.2018.06.023
12 C. J. Willmott: Phys. Geogr. **2** (1981) 184. https://doi.org/10.1080/02723646.1981.10642213
13 P. D. Bates, M. S. Horritt, and T. J. Fewtrell: J. Hydrol. **387** (2010) 33. https://doi.org/10.1016/j.jhydrol.2010.03.027
14 K. R. Dyer: Estuaries: A Physical Introduction (John Wiley & Sons, London, 1973). https://books.google.com/books?id=_8hRAAAAMAAJ
15 J. T. Morris, P. V. Sundareshwar, C. T. Nietch, B. Kjerfve, and D. R. Cahoon: Ecology **83** (2002) 2869. https://doi.org/10.1890/0012-9658%282002%29083%5B2869%3AROCWTR%5D2.0.CO%3B2
16 M. E. Scully and C. T. Friedrichs: J. Geophys. Res. Oceans **112** (2007) C07028. https://doi.org/10.1029/2006JC003784
17 C. A. Ruhl and D. H. Schoellhamer: San Franc. Estuary Watershed Sci. **2** (2004) 1. https://doi.org/10.15447/sfews.2004v2iss2art1
18 E. A. Lee, S. Y. Kim, and H. S. Min: Tellus A: Dyn. Meteorol. Oceanogr. **71** (2019) 1604058. https://doi.org/10.1080/16000870.2019.1604058
19 R. Soulsby: Dynamics of Marine Sands: A Manual for Practical Applications (Thomas Telford, London, 1997). https://doi.org/10.1680/doms.25844
20 Monthly People: EGIS Enables Prediction of Suncheon Bay Wetland Development Using a Digital Twin (in Korean) https://www.monthlypeople.com/news/articleView.html?idxno=700767 (accessed June 2026).

About the Authors

Jun-Ho Lee received his B.S. degree in environmental science from Hankuk University of Foreign Studies, Republic of Korea, in 2003, and his M.S. and Ph.D. degrees in environmental science (marine environment) from the same university in 2005 and 2012, respectively. He has been with the Korea Institute of Ocean Science and Technology (KIOST) since 2005, where he has conducted research on marine geology, coastal sedimentology, and estuarine environments. He is currently the director of the Korea–Peru Joint Research Center on Ocean Science and Technology for Latin America (KOPELAR). His research interests include estuarine and coastal sedimentology, tidal-flat morphodynamics, marine environmental monitoring, digital-twin technologies, and integrated coastal management. (leejh@kiost.ac.kr)

Keunyong Kim received his M.S. degree in ocean ecology and Ph.D. degree in marine ecology by remote sensing from Chonnam National University, Korea, in 2009 and 2015, respectively. Since 2017, he has been a senior research scientist with the Korea Ocean Satellite Center, Korea Institute of Ocean Science and Technology (KIOST), Busan, Korea. His research interests include marine disaster and change monitoring of the coastal environment. (keunyong@kiost.ac.kr)

Jingyo Lee received his B.S. and M.S. degrees in marine biology from Chosun University, Republic of Korea, in 2011 and 2016, respectively. He is currently pursuing his Ph.D. degree in the Department of Ocean Science and Technology Convergence at Korea Maritime & Ocean University (KMOU). He has been involved in research at the Korea Institute of Ocean Science and Technology (KIOST), with a focus on coastal remote sensing, tidal-flat geomorphology, and satellite-based environmental monitoring. His research interests include tidal-flat DEM reconstruction, long-term coastal topographic change analysis, optical satellite remote sensing, GIS-based spatial analysis, and integrated coastal management. (jingyo@kiost.ac.kr)

Hwangki Lee received his B.S., M.S., and Ph.D. degrees in naval architecture and ocean engineering from Chonnam National University, Republic of Korea, in 2014, 2016, and 2024, respectively. He has been with the Coast and Ocean Technology Research Institute Co., Ltd. since 2018, where he has conducted research on hydrodynamic and wave modeling, as well as AI-based wave overtopping prediction. He is currently a general manager at the company. His research interests include physical oceanography, AI, and numerical modeling. (hkl8809@cotri.co.kr)

Hoi-Soo Jung received his B.S., M.S., and Ph.D. degrees in oceanography from Seoul National University, Republic of Korea, in 1985, 1987, and 1994, respectively. He has been with the Korea Institute of Ocean Science and Technology (KIOST) since 1994 and is currently a principal research scientist. He previously served as director of the Korea–China Joint Ocean Research Center (JORC) in Qingdao, China, and deputy director of the International Cooperation Department at KIOST. He has published over 60 SCI(E)-indexed journal papers and has received more than 3400 citations on Google Scholar (as of February 20, 2024). His research interests include marine geology, sedimentology, coastal environments, and international cooperation in ocean science. (hsjung@kiost.ac.kr)